Three-Dimensional Self-Assembled Monolayer (3D SAM) of *n*-Alkanethiols on Copper Nanoclusters

T. P. Ang,[†] T. S. A. Wee,[‡] and W. S. Chin*[,†]

Department of Chemistry, National University of Singapore, 3, Science Drive 3, Singapore 117543, and Department of Physics, National University of Singapore, 2, Science Drive 3, Singapore 117542

Received: March 4, 2004

Three-dimensional self-assembled monolayer (3D SAM) of 1-octanethiol, 1-decanethiol, and 1-dodecanethiol has been formed on copper nanoclusters. The morphology and spectroscopy of the nanoparticles were characterized while the conformation of the 3D SAMs was investigated with thermal and variable-temperature analyses. TEM results suggest the copper clusters consist of a spherical shape of ∼3−5 nm. IR, XPS, and ^{13}C CPMAS NMR results confirm that alkanethiols are chemisorbed via the −SH group and the packing density of the alkanethiols on copper nanoclusters increases with the alkyl chain lengths. The thiol chain is deduced to adopt the all-trans zigzag conformation through the analysis by IR and ^{13}C CPMAS NMR. Low-angle peaks observed in XRD further suggest strong interdigitation among these chains to form superlattice structures. On increasing temperature, VT-FTIR and VT-^{13}C CPMAS NMR depict the disruption of lateral interaction between the chains. This melting of crystalline packing is endothermic but an exothermic peak was observed upon reheating in DSC. We attribute this exothermic "crystallization" to the conformational memory effect of the compact chains. We have found that much higher melting points and enthalpies are obtained on copper nanoclusters as compared to earlier reports on gold and silver clusters.

Introduction

Nanometer-sized metal particles possess novel properties due to quantum size confinement effects.[1] Deviation from bulk properties has made them interesting candidates for fundamental studies and potential new applications.[2] Among the many metallic elements, copper has shown promising catalytic ability to convert methanol and ethanol to aldehyde[3,4] while micro-copper particles have been employed in chemically modified electrodes for the detection of amino acids and polyhydric molecules.[3,5] Nonetheless, reports on copper nanoparticles are by far fewer compared to its gold and silver counterparts, mainly due to its susceptibility toward oxidation. Pileni et al.[6a,b] have demonstrated the synthesis of copper nanoparticles in reversed micelles and noted that their stability is adversely affected by the water content, leading sometimes to a layer of oxide formation.

Sols of metallic nanoparticles have long been prepared in colloidal solutions by reducing metallic ions in suitable solvents in the presence of some stabilizers.[1,7] Many metallic colloids of controlled sizes have been prepared with this approach, but the nanoparticles are not isolable from the solutions and hence could not be conveniently investigated and applied. In another aspect, self-assembled monolayers (SAMs) of long-chain alkanethiols have been studied extensively on metallic surfaces.[8] These organic chains were found to spontaneously self-organize, interact with each other via van der Waals forces, and form a compact monolayer that protects the underneath metal from the ambient. Despite the large surface curvature of the near-spherical particles, alkanethiols have been found to form compact monolayers on metallic nanoparticles,[9−12] named as "3D SAMs" by Hostetler et al.[10b] Such encapsulation with SAMs has allowed the monolayers to be studied by a host of analytical techniques that are difficult to apply to 2D monolayers. In addition, evidence showing interdigitation between monolayer-protected Ag nanoparticles to form superlattices has been reported recently.[11]

The 3D SAMs studies have thus far been confined to both gold and silver nanoparticles. In this paper, we present a thorough study on 1-octanethiol (C8), 1-decanethiol (C10), and 1-dodecanethiol (C12) capping on copper nanoparticles as the protecting groups. Chen et. al. have recently reported a study on hexanethiol-protected copper nanoclusters,[12a] but did not observe the formation of 3D SAMs of the adsorbed hexanethiol on the nanoclusters. We estimated that a more compact monolayer could be formed using longer chains, and also on copper nanoclusters compared to its gold and silver analogues.[8c] For the first time, we report the melting behavior of these 3D SAMs as shown by thermal analysis and various variable-temperature techniques.

Experimental Section

Materials. Copper(II) nitrate hemipentahydrate (98%) was obtained from Sigma-Aldrich and 1-dodecanethiol (98%) was obtained from Acros Organic. 1-Octanethiol (97%), 1-decanethiol (95%), and sodium borohydride (96%) were from Fluka. All reagents and solvents were used as received. Milli-Q purified water was used throughout the preparation.

Preparation. The thiolated copper nanoclusters were synthesized in solution by using a modified literature method reported originally for silver clusters.[11a] About 0.450 g of copper(II) nitrate was first dissolved with ∼120 mL of absolute alcohol in a round-bottomed flask and the respective alkanethiol

* Author to whom correspondence should be addressed. E-mail: chmcws@nus.edu.sg.
[†] Department of Chemistry, National University of Singapore.
[‡] Department of Physics, National University of Singapore.

10.1021/jp049006r CCC: $27.50
Published on Web 06/25/2004

(1:1 molar ratio to Cu) was added with stirring. About six times the molar solution of sodium borohydride in ethanol was then added dropwisely into the reaction mixture. The reaction was maintained at room temperature with vigorous stirring for 2 h. The entire reaction was purged and carried out in an inert N_2 atmosphere to prevent oxidation of copper. A brownish precipitate was isolated by centrifugation, washed repeatedly with deionized water, toluene, ethanol, and acetone, and vacuumed dried. The stored samples were found to be stable up to at least 6 months, with only a very small increase in the oxygen content as shown by XPS analysis.

Characterization. The surface chemical composition of the copper nanoclusters was analyzed with a VG Scientific ESCALAB MK II operated at 120 W. A monochromatic Mg Kα X-ray source at 1253.6 eV was used, and the system was calibrated with respect to the Cu 2p peak from a standard sample ($CuSO_4 \cdot 5H_2O$). The crystal phase of the nanoclusters was analyzed with a Siemens X-ray diffactometer (D5005) operated at 40 kV and 40 mA. Solid-state CPMAS ^{13}C NMR and variable-temperature CPMAS ^{13}C NMR spectra were recorded with a Bruker DRX 400 MHz spectrometer with the spin rate of 8000 per second. Infrared (IR) spectra were recorded on a KBr disk with a Bio-rad FT-IR spectrometer FTS 165. Elemental analyses were performed with a Thermo Jarrell Ash IRIS AP Duo inductively coupled-optical emission spectrometer and a Perkin-Elmer PE 2400 CHNS elemental analyzer.

The size and morphology of the nanoclusters prepared were determined by transmission electron microscopy (TEM). A drop of nanoclusters dispersed in toluene was placed on a copper grid coated with a thin film of Formvar and dried. Electron micrographs were taken with a JEOL LEM-100CXII electron microscope at an accelerating voltage of 100 kV. The particle sizes were determined from the maximum length of the particles.

The desorption temperature of the adsorbed alkanethiols and the percentage weight loss of the nanoclusters were determined with a TA Instruments SDT 2960 Simultaneous DTA-TGA analyzer under nitrogen (flow rate = 70 mL/min) at a heating rate of 20 deg/min. Differential scanning calorimetry (DSC) was performed with a TA Instruments DSC 2920 Calorimeter under nitrogen (flow rate = 100 mL/min) at a heating rate of 10 deg/min.

Results and Discussion

To facilitate discussion, the nanocluster samples are abbreviated with the number of carbon atoms in the alkanethiol chain, i.e., Cu−C8 for octanethiol-capped, Cu−C10 for decanethiol-capped, and Cu−C12 for dodecanethiol-capped copper nanoclusters, respectively.

All three samples prepared are brown-colored powders that are not soluble in most common solvents after drying. Figure 1 depicts typical TEM images and the size histograms of the samples redispersed in toluene and dropped-cast onto copper grid. Generally, some individual spherical nanoparticles can be seen together with some larger clusters under the microscope. Average sizes of the dispersed particles are estimated to be ~3−5 nm. The average sizes seem to be decreasing for copper clusters capped with longer alkanethiol chain, although the difference is not that significant. We will discuss the results of various spectroscopic and thermal analyses of these samples in the following sections.

(A) Spectroscopic Analysis. *XPS Analysis.* The compositions of the samples were first checked with XPS analysis. Figure 2 depicts typical XPS spectra of the nanoclusters over the full range and the individual elemental photoelectron peaks. For all samples, the oxygen peak (~530 eV) is either not detected or only observed in insignificant amounts. This clearly confirms that these C8−C12 alkanethiols could form a good barrier layer that protects the copper cores from oxidation. The stability of this protective layer is significant, as verified by just a small increase in the O 1s signal after 6 months of storage at ambient conditions (inset in Figure 2).

TABLE 1: XPS Analysis of the Thiolated Copper Nanoclusters: Binding Energy (BE, eV), Relative Peak Intensity (RPI, %), and Relative Atomic Ratio (RAR) Normalized to Sulfur

		Cu−C8		Cu−C10		Cu−C12	
	BE (eV)	RPI (%)	RAR	RPI (%)	RAR	RPI (%)	RAR
C 1s	284.8	100	8.1	100	11.1	100	14.8
S $2p_{3/2}$	162.4	67.2	1	66.8	1	67.2	1
S $2p_{1/2}$	163.6	32.8		33.2		32.8	
Cu $2p_{3/2}$	932.3	69.7	1.2	71.7	1.2	69.7	0.9
Cu $2p_{1/2}$	952.1	30.3		28.3		30.3	

In their study on alkanethiol 2D SAMs on copper, Laibinis et al. monitored the intensity of Cu(II) XPS peak to follow the rate of oxidation of copper.[13] The presence of charge-transfer shake-up satellite alongside the Cu $2p_{3/2}$ and $3s_{1/2}$ peaks is well-documented for copper(II) compounds.[14,15] In our case, the Cu $2p_{3/2}$ peak is found at 932.3 eV (Table 1), about 1.5 eV lower than that typical of CuO, and the satellite structure is clearly not detected. This thus precludes any significant oxidation of the copper nanoparticles, certainly not in the form of CuO.

On the other hand, it is known that the typical $2p_{3/2}$ peak of Cu(0) is only ~0.1 eV away from that of Cu(I) species and a comparison with the $L_3M_{4,5}M_{4,5}$ Auger transition is normally used to distinguish the two species.[16] By correlating our values of Cu $2p_{3/2}$ and the LMM Auger peak positions,[16c] however, we found that the valence state of Cu in our samples lies between 0 and +1. This is clearly not due to the formation of Cu_2O on the surface, since the O 1s peak is not significant. It is expected that the surface Cu atoms would acquired a $\delta+$ charge due to chemisorption of the alkanethiols. We perform DFT calculations using a simple model consisting of one copper atom bonded to a single thiolate chain, with the aim of gaining some insight on the Cu−S bond.

Through fully optimized energy minimization, B3LYP/6-31G calculations give an all-trans zigzag structure for all three thiolated clusters. One such structure for Cu−C12 is shown in Figure 3, together with the predicted atomic charges. Thus, DFT calculations predicted a positive charge of about + 0.5 on the copper atom bonded to the thiol group. The negative charge is distributed between the S and the α-C atoms, with the former acquiring about −0.4 and the latter about −0.1. This prediction agrees well with the $\delta+$ valence detected in XPS. The DFT-predicted Cu−S bond length is 2.096 Å, as compared to 2.147 Å reported for copper(I) aliphatic thiolate complexes.[17] The end-to-end lengths of the zigzag chain (i.e., linear distance from Cu to end-C) were calculated as 12.0, 14.6, and 17.1 Å for the C8, C10, and C12 thiolates, respectively.

The S $2p_{3/2}$ component that appeared at ~162 eV in the XPS spectra (Table 1) compares very well with the typical value of chemisorbed S species.[15] The slight downward shift relative to sulfur in free alkanethiols (163.5−163.8 eV)[15] is in agreement with the $\delta-$ charge predicted by the DFT calculations. The absence of sulfonate signal (typically appears at >167 eV)[15] further precludes the formation of any oxidized interface between the clusters and the 3D SAMs.

As seen in Table 1, the C:S atomic ratios were found to be slightly higher than those expected from the respective free

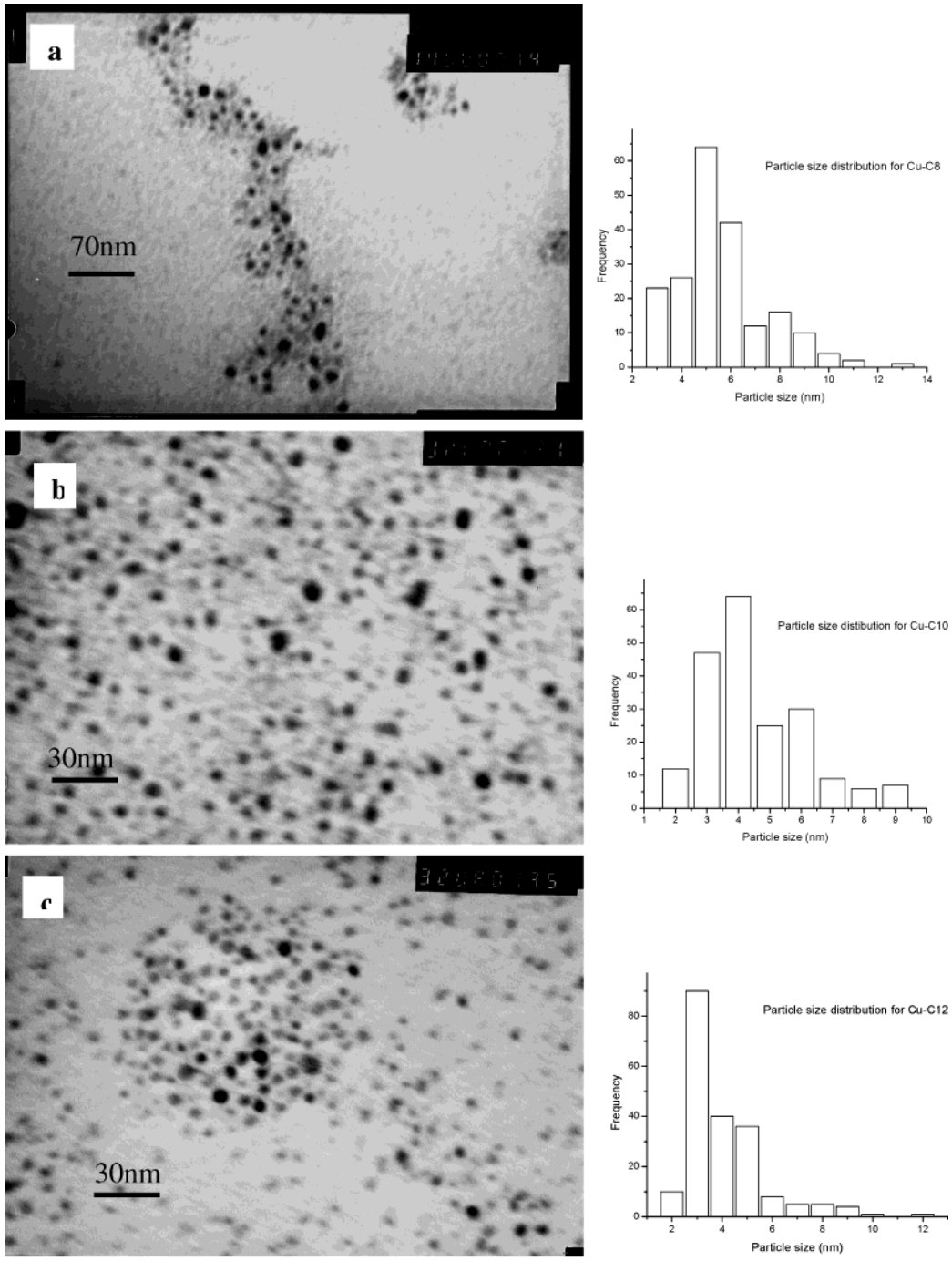

Figure 1. TEM images of the various thiolated copper nanoclusters (a) Cu−C8, (b) Cu−C10, and (c) Cu−C12, with histograms showing the respective size distribution.

alkanethiols. This is not uncommon, as is normally attributable to carbonaceous contamination. On the other hand, the Cu:S ratio is 1.2 for both the Cu−C8 and Cu−C10 clusters, but reduces to 0.9 for the Cu−C12 clusters. This suggests that more C12 thiols are adsorbed onto the Cu nanoclusters compared to the shorter C8 and C10 thiols.[8a] Since TEM analysis indicated slightly smaller particle size for Cu−C12, this would mean that the packing of 1-dodecanethiol is denser on the copper surface.

Transmission IR Spectra. The transmission IR spectra of the various thiolated nanoclusters (KBr pellets) over the high- and low-frequency regions are shown in Figure 4. Comparing with the respective free alkanethiols, three significant differences are noted, i.e., (i) the S−H stretching band at 2550−2600 cm^{-1} is absent in the spectra of the nanoclusters, (ii) the CH_2 symmetrical and asymmetrical stretching bands appear at lower wavenumbers compared to the respective free alkanethiols, and (iii) progression bands are clearly observed only in the spectra of the nanoclusters.

The absence of the S−H stretching band is expected since the S−H bond is broken upon chemisorption onto the nanoclusters. On the other hand, the symmetrical (d^+) and asymmetrical (d^-) CH_2 stretching vibrations are commonly used as an indicator for the degree of ordering (crystallinity) of the alkyl chains.[18,19] The frequencies for crystalline polyethylene or typical all-trans zigzag conformations are usually below 2850 and 2920 cm^{-1} respectively. Thus, a shift to lower wavenumbers from the free thiols suggests that the chemisorbed alkanethiol species is more ordered on the surfaces of these copper nanocrystals, and probably adopts an all-trans zigzag conformation.

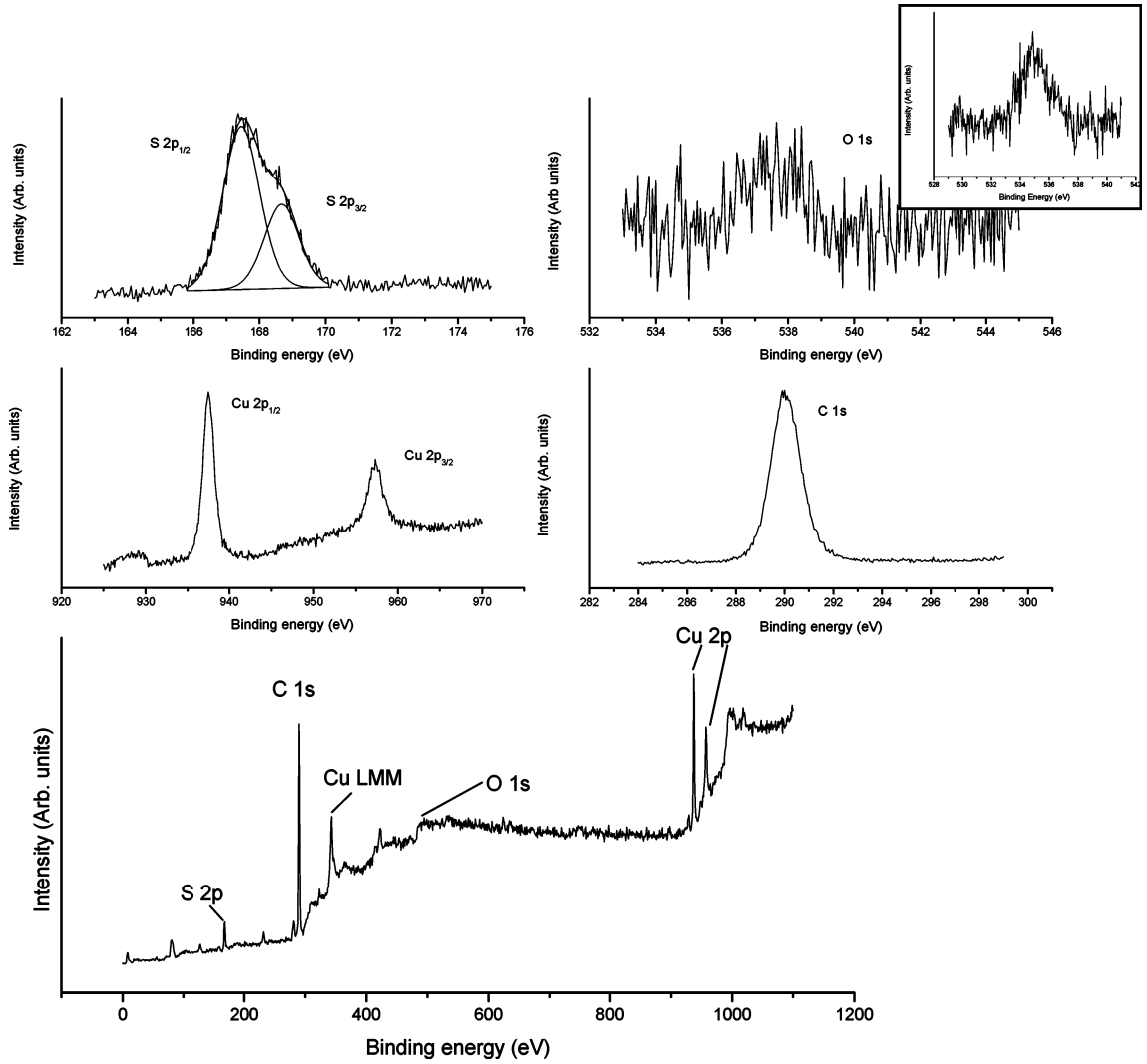

Figure 2. Typical XPS spectrum of thiolated copper nanoclusters (Cu−C12 shown here). Inset: The O 1s signal after 6 months of storage at ambient conditions.

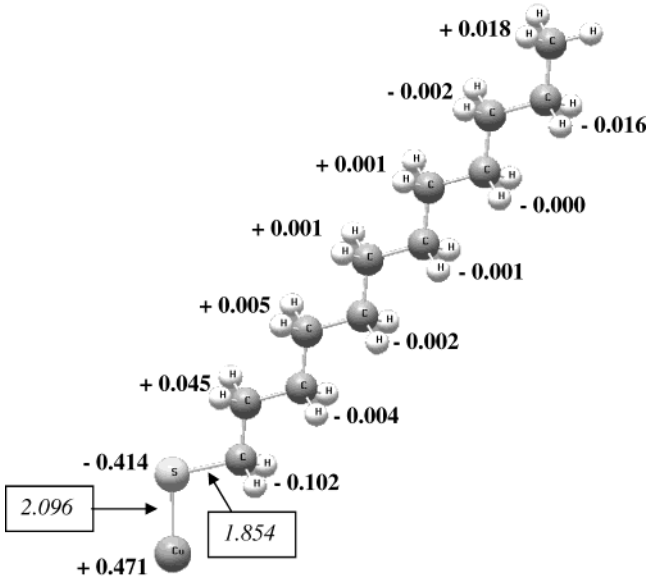

Figure 3. B3LYP/6-31G(d,p) optimized structure for the Cu−C12 cluster. Numbers in bold are the atomic charges predicted for the heavy atoms. Numbers in boxes are the calculated bond lengths.

The well-resolved progression bands in the 1150−1400-cm^{-1} region can be assigned to the twisting-rocking (T_x) and wagging (W_x) progression bands. These bands are also used as a strong indicator of crystallinity,[10b,20] thus implying that alkanethiol species are ordered when chemisorbed onto the copper nanoclusters. Some chain defects are expected, especially from the end-rotation of the longer chains. Thus, peaks at ∼1341 and ∼1081 cm^{-1} are assigned to the end-gauche conformation.[10b]

NMR Spectra. To further investigate the local environment of the thiol chains on the nanoclusters, we have measured their CPMAS ^{13}C NMR spectra as displayed in Figure 5. For comparison, the ^{13}C NMR spectrum of 1-dodecanethiol monomer in $CDCl_3$ is included in the inset. The assignment of the various carbon sites has been carried out in comparison with those reported for alkanethiol monomers and the thiolated gold clusters.[21] Table 2 summarizes the chemical shift values and the respective assignment. The carbon numbering is depicted at the upper right corner of Figure 5.

In Table 2, we can clearly see that resonances of the dodecanethiol carbons are shifted downfield systematically upon chemisorption in the Cu−C12 sample. This downfield shift is particularly large (∼17 ppm) for the C1 atom, and becomes smaller away from the copper/sulfur interface to a value of ∼0.2 ppm for the C12 atom. Such a significant downfield shift on C1 rules out the possibilities of weakly associated organosulfur species (possible impurities in the preparation), air-oxidized species, or physisorbed species.[10e] It

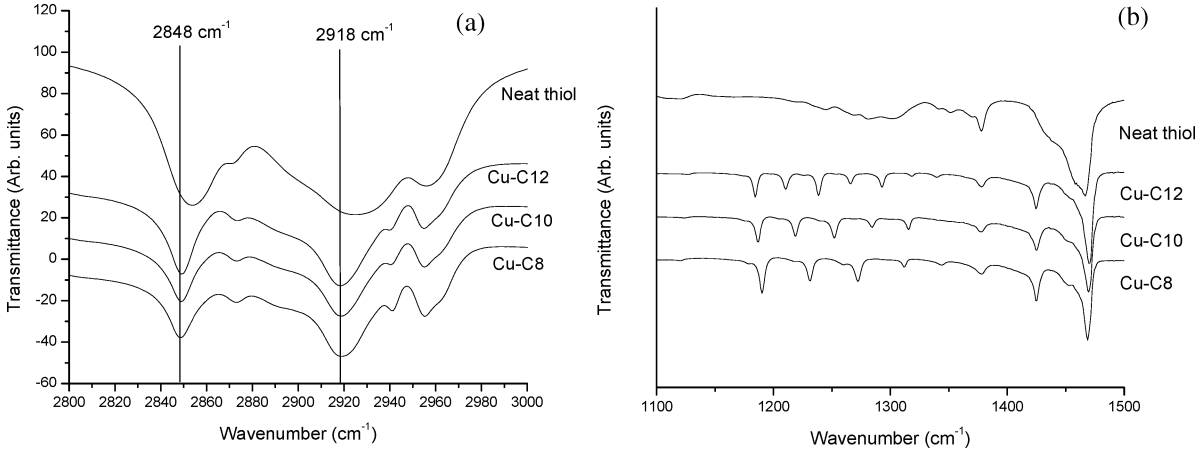

Figure 4. (a) The symmetrical and asymmetrical methylene C−H stretching vibrations and (b) the progression peaks detected for thiolated nanoclusters. The IR spectrum of neat dodecanethiol is included for comparison.

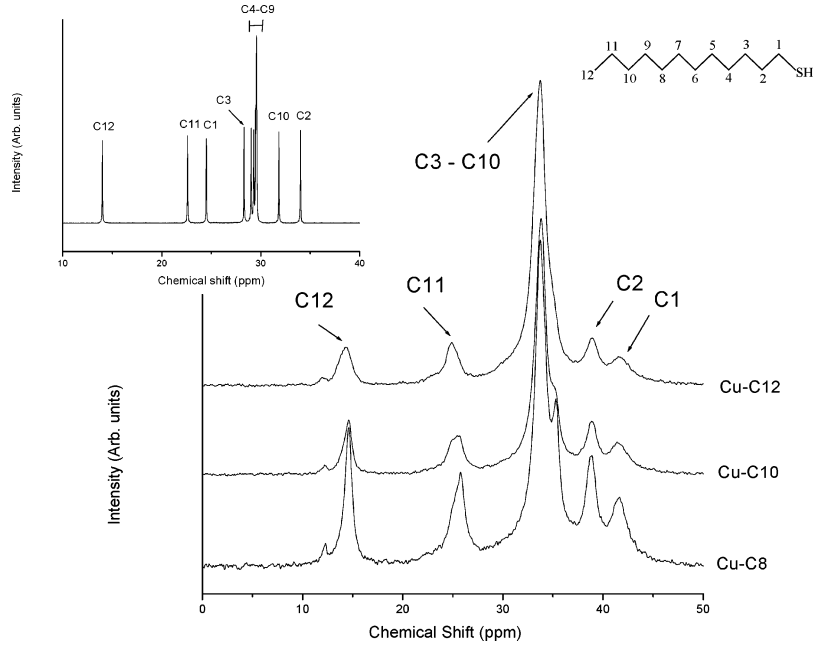

Figure 5. CPMAS ^{13}C NMR spectra of the thiolated nanoclusters. The inset shows the ^{13}C NMR spectrum of dodecanethiol monomer. The carbon numbering is depicted at the upper right corner.

TABLE 2: Chemical Shift Values (δ, ppm) and the Assignment of the Various Carbon Sites

Cu−C8		Cu−C10		Cu−C12		dodecanethiol	
C	δ	C	δ	C	δ	C	δ
1	41.6	1	41.4	1	41.5	1	24.5
2	38.9	2	38.8	2	38.9	2	34.0
3−5	31.7−34.9	3−8	31.7−35.7	3−10	31.3−35.6	3−9	28.3−29.6
6	35.3					10	31.8
7	25.8	9	25.4	11	24.9	11	22.6
8	14.6	10	14.6	12	14.2	12	14.0

confirms that the Cu−S interaction takes the form of the copper−thiolate chemisorbed bond.

In addition, the downfield shift is also an indication that the thiol chains are conformationally ordered.[21] For bulk *n*-alkanes in the crystalline state, carbon resonances are reported at 33−34 ppm, as compared to resonances at 29−30 ppm in the solution.[21] Such a downfield shift in chemisorbed alkanethiols can thus be attributed to a more crystalline all-trans conformation, in contrast to equal populations of trans and gauche conformations in the liquid free thiols. Conduction electrons from the metal core do not contribute much to the large downfield shift in C1, as has been confirmed by Badia et al. in a relaxation study on thiolated gold nanoclusters.[21]

Differences in chemical shift values are not significant among the three copper nanoclusters, but one can observe a trend of increasing peak width with the chain length. Such a peak broadening is exemplified most clearly from the gradual disappearance of the shoulder peak at ∼35 ppm from Cu−C8 to Cu−C12. The peak broadening effect was reported in other studies,[10a,c−f] and some attributed it to the fast spin relaxation from mutual dipolar interaction among the ordered chains.[10f] Since the C1 atom is closest to the copper/sulfur interface and is the most densely packed, it is thus expected to give the broadest peak. Comparatively, the terminal methyl carbons (e.g. C12 in Cu−C12) will have the highest orientation degree of freedom. They will hence experience the slowest spin relaxation and give the slenderest peak. Thus, the increase in peak width from Cu−C8 to Cu−C12 seems to suggest stronger dipolar interactions and thus a more ordered chain arrangement in the latter. Alternatively, the highly faceted surfaces of the nanoclusters can also lead to peak broadening by providing multiple binding sites for the thiols.[10e] Different chemisorption sites on the clusters, e.g. the faces, edges, and corners, will give rise to

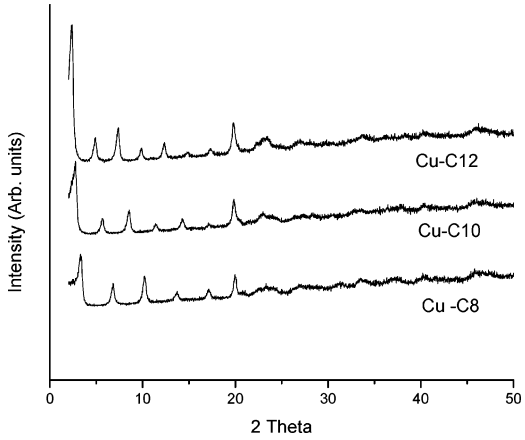

Figure 6. X-ray powder diffractograms of Cu−C8, Cu−C10, and Cu−C12 samples.

TABLE 3: Indexing for the Low-Angle XRD Peaks

Cu−C8		Cu−C10		Cu−C12	
2θ	(*hkl*)	2θ	(*hkl*)	2θ	(*hkl*)
3.3	(111)	2.8	(111)	2.4	(111)
6.8	(222)	5.6	(222)	4.9	(222)
10.2	(333)	8.6	(333)	7.3	(333)
13.6	(710)	11.5	(710)	9.8	(700)
17.2	(654)	14.2	(662)	12.4	(662)
20.1	$(\bar{1}06\bar{2})$	17.2	$(\bar{1}03\bar{1})$	14.8	$(\bar{1}02\bar{2})$

a distribution of chemical shift values. We believe the contribution of these multiple binding sites to peak broadening is significant, as suggested by the thermal analysis results discussed in subsection B.

XRD Analysis. Figure 6 presents the powdered X-ray diffractograms of the Cu nanoclusters. While peaks due to fcc copper metal[6c] are not detected, low-angle peaks are similarly observed for all three copper nanoclusters. This suggests that some superlattice diffractions are present in these nanoclusters, similar to what was reported on silver.[7f,11b]

In Table 3, it was found that these peaks can be consistently indexed to face-centered cubic unit cells. The calculated edge lengths for the unit cell are 45.9, 54.8, and 62.9 Å for the Cu−C8, Cu−C10, and Cu−C12 nanoclusters, respectively. This superlattice formation is attributed to the interdigitaion (or intercalation) of alkanethiol chains chemisorbed on adjacent copper clusters; it is expected to be effective only if an all-trans conformation is adopted in these clusters. The edge lengths estimated from XRD clearly suggest interdigitation of several carbon units between two adjacent nanoclusters. In the following section, we investigate the effect of heat on the structures of these superlattices.

(B) Thermal Analysis. Figure 7 shows the TGA results and the first derivative of weight loss for the three samples. The desorption temperature, percentage weight loss, and calculated copper to thiol molar ratio are tabulated in Table 4.

A slight increase in desorption onset is observed with increasing thiol chain length in Table 4. Similar observation was previously reported by Terrill et al.[10a] and Sandhyarani et al.,[11b] although no explanation has been offered. From first principle, if we assume that the organic fragments are desorbing from the nanoclusters, this temperature should be indicative of the strength of chemisorption. But it seems unlikely that the three alkanethiols will show very different reactivity toward copper nanoclusters, indeed DFT calculations have predicted the same Cu−S bond length for these nanoclusters. We would hence suggest that the difference in desorption onset is due to the lateral van der Waals attraction between the chains, which is stronger for the longer chain alkanethiols.

We also noticed from the derivative thermographs (Figure 7b) that the weight loss is not a simple one-step process. First, a shoulder is observed at the higher temperature side of the main peak of Cu−C8. This shoulder grows higher in intensity in Cu−C10 and finally becomes the main peak in Cu−C12. For such a two-step desorption, it may be argued that fragmentation of the organics has occurred in a stepwise manner. On the other hand, consistent with other reports[11b] and our CPMAS ^{13}C NMR results above, the desorption could have occurred from different binding sites on the nanoclusters. Different binding sites will give rise to different local surface morphology for the formation of SAMs, and the chains will thus require a slightly different amount of energy upon desorption.

In Table 4, the percentage weight loss also increases with the chain length. This corresponds well with the increasing mass of the respective chains, and confirms that the loss is due to desorption of the organic fragments. We can thus estimate from the weight loss the relative molar ratio of organic to inorganic fragment. As shown in Table 4, similar alkanethiol coverage is estimated for the Cu−C8 and Cu−C10 samples, while slightly higher coverage of thiol chains is obtained for the Cu−C12 sample. This result agrees well with the XPS data in subsection A.

DSC analysis (Figure 8) also suggests differences among the three thiolated samples. As shown in Table 5, the melting point and melting enthalpy increase with the alkanethiol chain length. Since an all-trans conformation and interdigitation of chains are deduced from IR, NMR, and XRD analyses, disruption of interdigitation is expected to give an endotherm before the desorption peak. This may be referred to as the "melting" of the interdigitated crystalline structures.[10a,d] In principle, the melting point (i.e. the degree of interdigitation) and melting enthalpy (i.e. the amount of interdigitation) should provide a direct measure of the relative population of the trans conformation in the sample.[10a,c] The results in Table 5 thus suggest that the population of trans conformation increases from Cu−C8 to Cu−C12 samples.

Comparing with other reported DSC data, we notice that our samples give much higher melting points and enthalpies compared to, e.g., dodecanethiol-protected gold nanoclusters (3 °C and 7.7 J/g)[10a,c] and octadecanethiol-protected silver nanoclusters (66 °C and 107.9 J/g).[11b] This implies a much denser coverage and a more compact interdigitation of thiols on the copper analogue, as compared to those on gold and silver clusters. This result is consistent with that deduced from the study of 2D SAMs on gold, silver, and copper.[8c] We believe the high extent of chain interdigitation in this case has led to the insolubility of our copper nanoclusters in most common solvents. The highly compact SAMs on the surface is also partly responsible for the absence of the copper surface plasmon peak at 556 nm in our absorption spectra.[6d]

When we performed a repeat run of DSC on a preanalyzed sample, we found that an exothermic peak (labeled as T_{exo} in Figure 9) appeared for all the nanoclusters before their melting points. Such an exothermic peak is not present in the first DSC run and has not been reported before in other 3D SAMs studies. In the following section, we attempt to gain an insight into the nature of this exothermic peak using variable-temperature (VT) studies.

(C) Variable-Temperature Studies. We first study the behavior of SAMs using VT-IR analysis. For simplicity, we

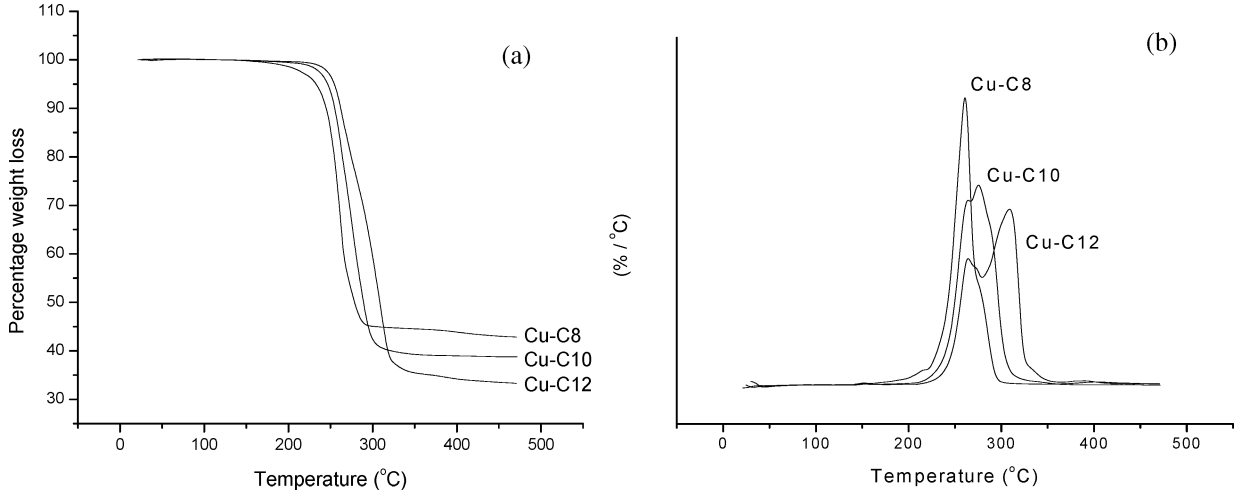

Figure 7. (a) TGA and (b) the first derivative thermographs of the thiolated nanoclusters.

TABLE 4: Desorption Temperature Onset, Percentage Weight Loss, and the Molar Ratio of Copper to Thiol[a]

samples	Cu−C8	Cu−C10	Cu−C12
desorption temp onset (°C)	245	249	264
wt loss (%)	57.1	61.2	66.7
molar ratio of copper to thiol[a]	1.7:1	1.7:1	1.6:1

[a] Estimated by assuming (i) the weight residue after analysis is pure copper in the nitrogen environment and (ii) the total weight loss corresponds to the desorption of alkanethiol only, e.g., for Cu−C8 the mole fraction of thiol = 57.1 ÷ 145.0 = 0.394, the mole fraction of copper = 42.9 ÷ 63.6 = 0.675, and molar ratio = 0.675:0.394 = 1.7:1.

TABLE 5: Melting Points and Enthalpies of the Thiolated Copper Nanoclusters

sample	mp (°C)	melting enthalpy (J/g)
Cu−C8	145.7	116.8
Cu−C10	146.2	119.9
Cu−C12	148.4	130.8

will focus our discussion on Cu−C12, although similar results have been obtained for the Cu−C8 and Cu−C10 samples. Figure 10 illustrates the variations of d^+ and d^- methylene C−H stretching vibration with temperature.

On increasing temperature, both stretching vibrational modes gradually shift toward higher wavenumber until a sharp increase is noted near the melting point (T_m = 148.4 °C for Cu−C12). As discussed in subsection A, such a shift to higher wavenumber is indicative of a less crystalline or more "liquid-like" chain behavior. This clearly suggests the disruption of the extended all-trans conformation, and thus the extent of interdigitation among the alkanethiol chains. It is believed that this disruption will continue as temperature is increased further and eventually lead to the maximum number of gauche conformations possibly present in the sample. The same observation has been reported for the gold[10c] and silver[10b] nanoclusters. Other evidence for the decrease of the all-trans population is given in Figure 11 by the gradual attenuation of the progression peaks as temperature increases.

In our repeat DSC analysis, an exothermic peak T_{exo} = 104.2 °C was detected when cooled Cu−C12 sample was reheated again. To understand the origin of this exothermic peak, we have subjected a Cu−C12 sample to ~220 °C (i.e. above T_m) at ambient and investigated the VT-IR behavior of the heat-treated sample. In Figure 12, the IR spectra of the sample before and after heat treatment are compared. It can be seen that a slight shift in the d^+ stretching from 2848 to 2851 cm^{-1} can be

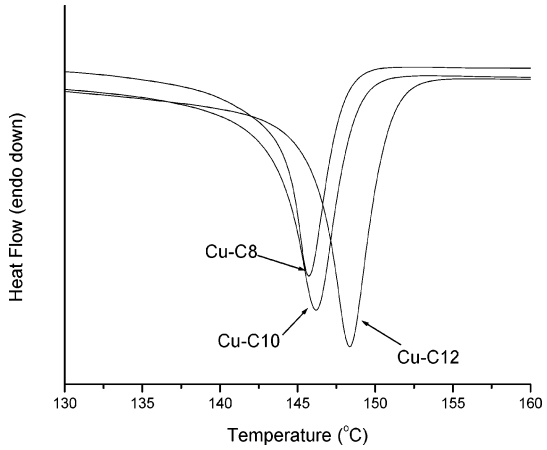

Figure 8. DSC endotherms of the thiolated copper nanoclusters.

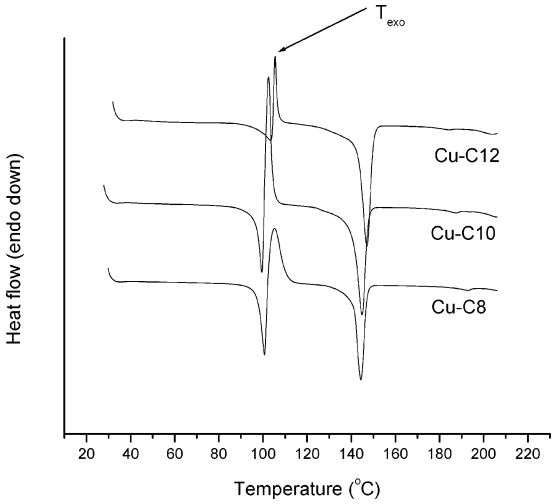

Figure 9. Repeat run of DSC on preanalyzed samples. Note that an exothermic peak (T_{exo}) can be observed at around 105 °C for all three samples.

detected for the heat-treated sample. In addition, the progression profile for the heat-treated sample is much less profound as shown in Figure 12b. This suggests that heat treatment has disrupted the ordered SAMs and hence more gauche conformation is now present in the sample.

We then follow the IR spectrum of the heat-treated Cu−C12 sample at different temperatures as presented in Figure 13. The

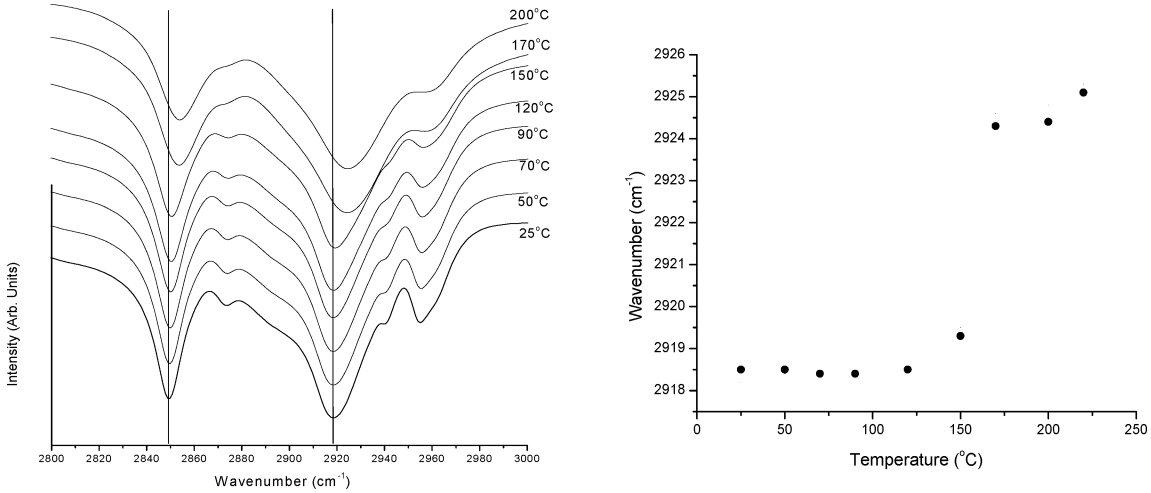

Figure 10. Variation of methylene symmetrical and asymmetrical C−H stretching vibrations of Cu−C12 sample with temperature. Right: The position of asymmetrical C−H stretch plotted against temperature.

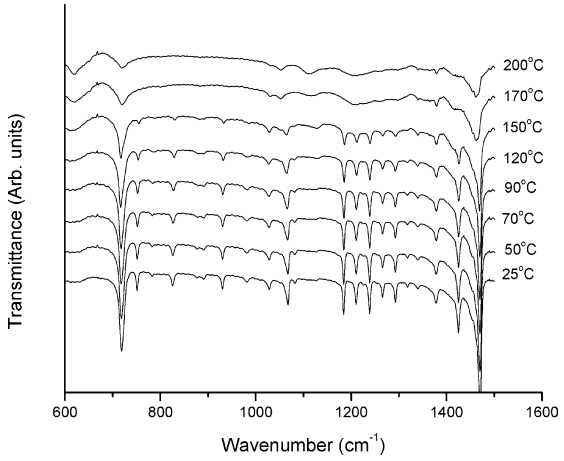

Figure 11. Variation of the progression peaks of Cu−C12 sample with temperature.

methylene d^+ C−H stretching vibration is seen to first shift toward lower wavenumber until around T_{exo}, then reverse its shift direction toward higher wavenumber. The result clearly suggests that the gauche conformation (resulting from the first heating cycle) is reverting back to the trans conformation near T_{exo} during the reheating process. Energy is released ("enthalpy of crystallization") during this conversion and it is exemplified as the exothermic peak at T_{exo}.

Such an exothermic peak has not been observed for gold and silver thiolated nanoclusters, and we believe our observation is mainly attributed to the very compact nature of SAMs on copper clusters. Thus, when the *trans*-alkanethiol chains were disrupted and transformed to gauche conformation during the first heating cycle, some chains "remember" their original conformation and revert back as soon as the sample is reheated. This "memory" phenomenon is possible due to the little available free volume surrounding these chains. In Figure 14, we illustrate this conversion with a schematic cartoon drawing.

It is also noted that, in Figure 12b, an additional peak at ∼1112 cm^{-1} is detected for the heat-treated Cu−C12 sample while the intensity of a peak at ∼620 cm^{-1} increases. The latter peak has been observed also by Hostetler et al.[10b] and was assigned to packing defects of alkanethiols on nanoclusters. The peak at ∼1112 cm^{-1}, however, is unknown. Although a similar position has been assigned to the trans C−C vibration,[10b] it is unlikely that such a trans conformation will be more pronounced in our heat-treated sample. We later confirmed from XPS analysis that a small oxygen peak as well as an emerging shoulder on the S 2p peak appeared for all the heat-treated samples. The shoulder that emerged on the S 2p peak can be peak-fitted at 161.3 eV and is probably due to species such as monosulfide or disulfide.[15] On the other hand, the presence of the oxygen peak indicates oxidation of the sample during heat treatment at ambient. Hence, the IR peak at ∼1112 cm^{-1} is probably due to the formation of oxidized carbon. A peak at a similar position has been reported for self-assembled oligo(ethylene glycol)-terminated and amide group-containing alkanethiol chemisorbed on gold, and it was assigned to the parallel-polarized C−O stretching mode.[17] Both the 620- and 1112-cm^{-1} peaks do not shift or change in intensity during the VT-IR analysis (Figure 13), thus confirming that these peaks do not play a part in the emergence of the exothermic peak in our repeat DSC study.

We have also performed a VT-^{13}C NMR study on the thiolated samples as shown in Figure 15. It is found that ^{13}C peaks due to the terminal carbons, i.e., C11 and C12, gradually sharpen as temperature increases. This is expected from the fact that the mobility of the chain ends increases with temperature and hence behaves more "liquid-like". In addition, temperature increase also sees the progressive manifestation of a peak at 30−31 ppm, which indicated the appearance of gauche conformation.[22] Hence, the observation in VT-^{13}C NMR confirms the increasing amount of gauche conformation with temperature. Unfortunately, we are unable to observe further variation at the melting transition (T_m) due to instrumental limitation.

Conclusion

In summary, we have studied several thiolated copper nanoclusters prepared via a liquid-phase method and investigated the 3D SAMs of the alkanethiol chains chemisorbed on the nanocluster surfaces. TEM analysis shows that spherical nanoparticles of ∼3−5 nm are produced, although the fcc copper peak in XRD and the surface plasmon absorption band of copper are not detected. We have found that this is mainly due to the very compact formation of SAMs on the copper nanoclusters, and indeed evidence of chain-interdigitation between neighboring clusters is clearly suggested by XRD and thermal analysis. It is known that such interdigitation would be possible if most of the alkanethiol chains adopt an extended all-trans conforma-

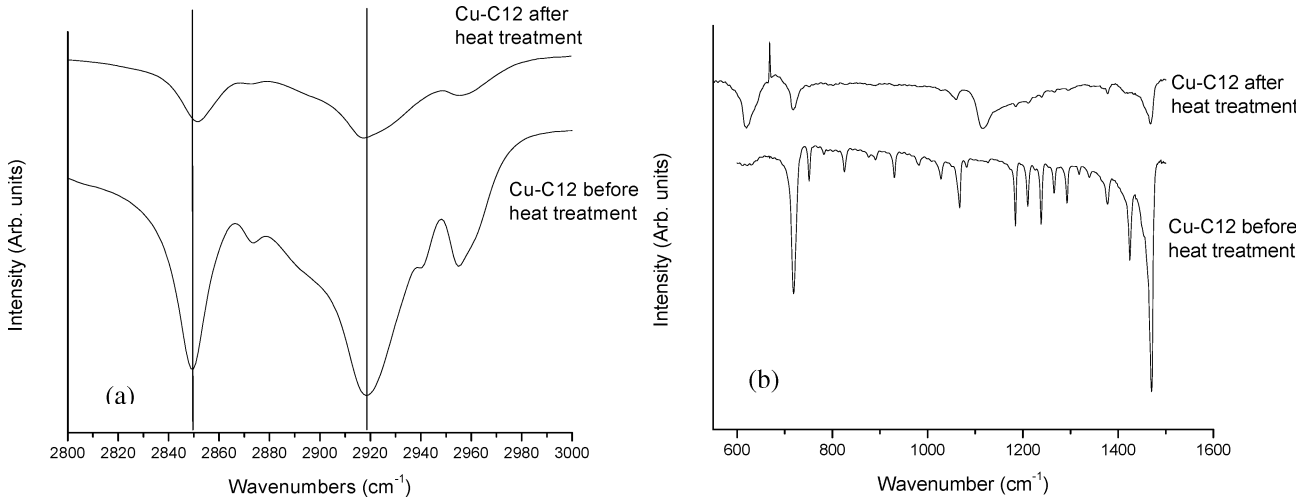

Figure 12. IR spectra of Cu−C12 before and after heat treatment: (a) methylene symmetrical and asymmetrical C−H stretching vibrations and (b) the progression peaks.

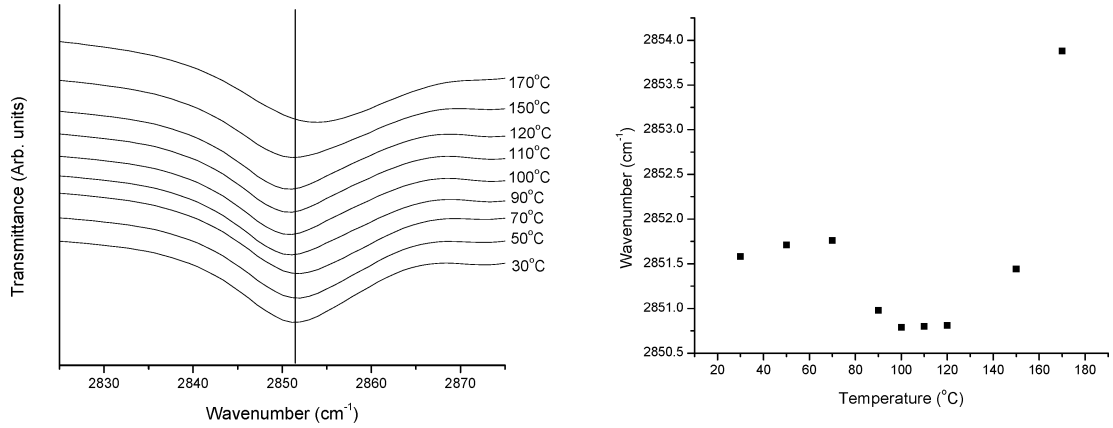

Figure 13. Variation of the symmetrical methylene C−H stretching vibration of a preheated Cu−C12 sample with temperature. Right: Wavenumber plotted against temperature.

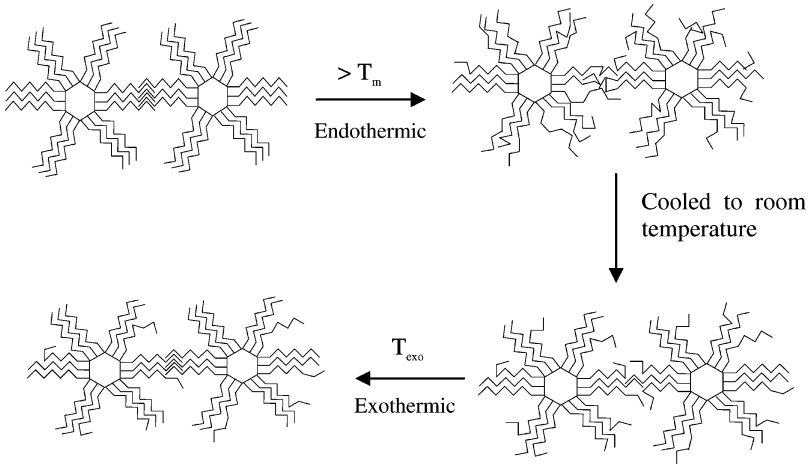

Figure 14. A schematic illustration of the melting behavior of the alkanethiol chains: some gauche conformations are retained after the heat treatment at T_m; on a repeat heating, the thiol chains crystallize again and exhibit an exothermic peak at T_{exo}.

tion. This deduction has been generally supported by our FTIR, CPMAS ^{13}C NMR, and DSC studies. XPS and TGA data also suggest that the coverage of alkanethiol increases with the thiol chain length, probably due to stronger lateral interactions between the longer chemisorbed chains.

Upon heating, the extended all-trans conformations of the alkanethiol chains are disrupted. A phase transition (T_m) involving conversion of such conformation to a more disordered gauche conformation is detected in DSC, VT-IR, and VT-CPMAS ^{13}C NMR analyses. An exothermic peak was observed at temperatures lower than T_m when heating is repeated on a pre-heat-treated sample. This observation is unprecedented and VT-IR analysis suggests that energy is released ("enthalpy of crystallization") when the conformational freedom resulting from

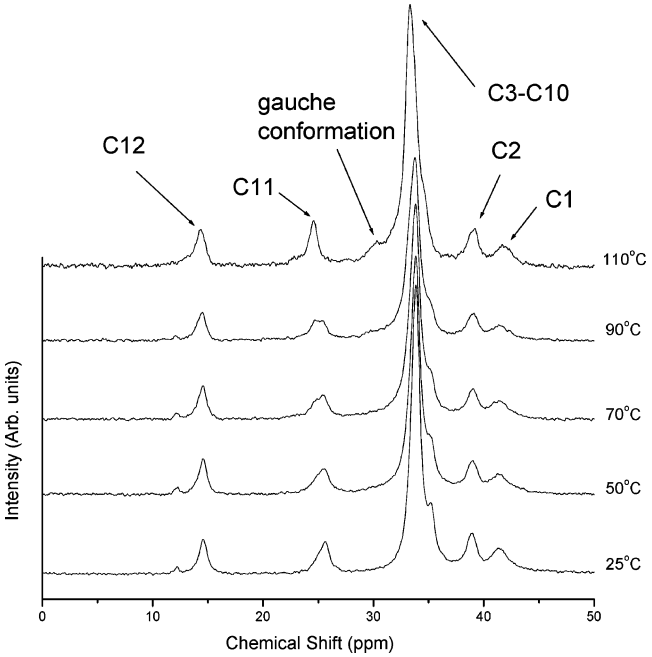

Figure 15. Variable-temperature CPMAS ^{13}C NMR spectra for Cu−C12.

the first heating cycle is lost, i.e., the chains partially revert back to the all-trans conformation for favorable interdigitation interactions.

Acknowledgment. This research work is supported by the National University of Singapore research grant (Grant No. R-143-000-123-112). We thank Mr. Wong Chiong Teck for his help in the DFT calculations.

References and Notes

(1) Henglein, A. *Chem Rev.* **1989**, *89*, 1861. (b) Schmid, G. *Chem. Rev.* **1992**, *92*, 1709.

(2) See, for example: Feldheim, D. L.; Foss, C. A., Jr., Eds. In *Metal Nanoparticles—Synthesis, Characterization and Applications*; Marcel Dekker: New York, 2002.

(3) Chen, T. Y.; Chen, S. F.; Sheu, H. S.; Yeh, C. S. *J. Phys. Chem. B* **2002**, *106*, 9717.

(4) (a) Bowker, M.; Madix, R. *J. Surf. Sci.* **1980**, 95, 190. (b) Bowker, M.; Madix, R. *J. Surf. Sci.* **1982**, *116*, 549.

(5) Casella, I. G.; Cataldi, T. R. I.; Guerrieri, A.; Desimoni, E. *Anal. Chim. Acta* **1996**, *335*, 217.

(6) (a) Tanori, J.; Pileni, M. P. *Langmuir* **1997**, *13*, 639. (b) Pileni, M. P.; Gulik-Krzywicki, T.; Tanori, J.; Filankembo, A.; Dedieu, J. C. *Langmuir* **1998**, *14*, 7359. (c) Arul Dhas, N.; Paul Raj, C.; Gedanken, A. *Chem. Mater.* **1998**, *10*, 1446. (d) Lisiecki, I.; Pileni, M. P. *J. Phys. Chem.* **1995**, *99*, 5077.

(7) (a) Brust, M.; Kiely, C. J. *Colloids Surf. A* **2002**, *202*, 175. (b) Sun, Y.; Xia, Y. *Science* **2002**, *298*, 2176. (c) Ung, T.; Liz-Marzán, L. M.; Mulvaney, P. *J. Phys. Chem. B* **2001**, *105*, 3441. (d) Crooks, R. M.; Zhao, M.; Sun, L.; Chechik, V.; Yeung, L. K. *Acc. Chem. Res.* **2001**, *34*, 181. (e) Templeton, A. C.; Wuelfin, W. P.; Murray, R. W. *Acc. Chem. Res.* **2000**, *33*, 27. (f) Whetten, R. L.; Shafigullin, M. N.; Khoury, J. T.; Schaaff, T. G.; Vezmar, I.; Alvarez, M. K.; Wilkinson, A.; *Acc. Chem. Res.* **1999**, *32*, 397. (g) Chen, S.; Huang, K.; Stearns, J. A. *Chem. Mater.* **2000**, *12*, 540.

(8) (a) Porter, M. D.; Bright, T. B.; Allara, D. L.; Chidsey, C. E. D. *J. Am. Chem. Soc.* **1987**, *109*, 3559. (b) Ulman, A.; Eilers, J. E.; Tillman, N. *Langmuir* **1989**, *5*, 1147. (c) Laibinis, P. E.; Whitesides, G. M.; Allara, D. L.; Tao, Y.-T.; Parikh, A. N.; Nuzzo, R. G. *J. Am. Chem. Soc.* **1991**, *113*, 7152. (d) Ihs, A.; Liedberg, B. *J. Colloid. Interface Sci.* **1991**, *144*, 282. (e) Uvdal, K.; Bodö, P.; Liedberg, B. *J. Colloid. Interface Sci.* **1992**, *149*, 162. (f) Laibinis, P. E.; Whitesides, G. M. *J. Am. Chem. Soc.* **1992**, *114*, 1990. (g) Keller, H.; Simak, P.; Schrepp, W.; Dembowski, J. *Thin Solid Film* **1994**, *244*, 799. (h) Jennings, G. K.; Munro, J. C.; Yong, T.-H.; Laibinis, P. E. *Langmuir* **1998**, *14*, 6130.

(9) (a) Brust, M.; Walker, M.; Bethell, D.; Schiffrin, D. J.; Whyman, M. *J. Chem. Soc., Chem. Commun.* **1994**, 801. (b) Sarathy, K. V.; Raina, G.; Yadav, R. T.; Kulkarni, G. U.; Rao, C. N. R. *J. Phys. Chem. B* **1997**, *101*, 9876. (c) Kang, S. Y.; Kim, K. *Langmuir* **1998**, *14*, 226. (d) Hosteler, M. J.; Zhong, C. J.; Yen, K. H.; Anderdgg, J.; Gross, S. M.; Evans, N. D.; Porter, M.; Murray, R. W. *J. Am. Chem. Soc.* **1998**, *120*, 9396 (e) Wuelfing, W. P.; Green, S. J.; Pietron, J. J.; Cliffel, D. E.; Murray, R. W. *J. Am. Chem. Soc.* **2000**, *122*, 11465.

(10) (a) Terrill, R. H.; Postlethwaite, T. A.; Chen, C. H.; Poon, C. D.; Terzis, A.; Chen, A.; Hutchison, J. E.; Clark, M. R.; Wignall, G.; Londono, J. D.; Superfine, R.; Falvo, M.; Johnson, C. S., Jr.,; Samulski, E. T.; Murray, R. W. *J. Am. Chem. Soc.* **1995**, *117*, 12537. (b) Hostetler, M. J.; Stokes, J. J.; Murray, R. W. *Langmuir* **1996**, *12*, 3604. (c) Badia, A.; Singh, S.; Demers, L.; Cuccia, L.; Brown, G. R.; Lennox, R. B. *Chem. Eur. J.* **1996**, *2* (3), 359 (d) Badia, A.; Cuccia, L.; Demers, L.; Morin, F.; Lennox, R. B. *J. Am. Chem. Soc.* **1997**, *119*, 2682. (e) Badia, A.; Demers, L.; Dickinson, L.; Morin, F. G.; Lennox, R. B.; Reven, L. *J. Am. Chem. Soc.* **1997**, *119*, 11104. (f) Hosteler, M. J.; Wingate, J. E.; Zhong, C. J.; Harris, J. E.; Vachet, R. W.; Clark, M. R.; Londono, J. D.; Green, S. J.; Stokes, J. J.; Wingnall, G. D.; Glish, G. L.; Porter, M. D.; Evans, N. D.; Murray, R. W. *Langmuir* **1998**, *14*, 17.

(11) (a) Murthy, S.; Bigioni, T.; Wang, Z. L.; Khoury, J. T.; Whetten, R. L. *Mater. Lett.* **1997**, *30*, 321 (b) Sandhyarani, N.; Resmi, M. R.; Unnikrishnan, R.; Vidyasagar, K.; Ma, S.; Anthony, M. P.; Selvam, G. P.; Visalakshi, V.; Chandrakumar, N.; Pandian, K.; Tao, Y. T.; Pradeep, T. *Chem. Mater.* **2000**, *12*, 104. (c) Sandhyarani, N.; Anthony, M. P.; Selvam, G. P.; Pradeep, T. *J. Chem. Phys.* **2000**, *113*, 9794.

(12) (a) Chen, S. W.; Sommers, J. M. *J. Phys. Chem. B* **2001**, *105*, 8816. (b) Kumar, R. V.; Mastai, Y.; Diamant, Y.; Gedanken, A. *J. Mater. Chem.* **2001**, *11*, 1209.

(13) Laibinis, P. E.; Whitesides, G. M. *J. Am. Chem. Soc.* **1992**, *114*, 9022.

(14) (a) Mclntyre, N. S.; Cook, M. G. *Anal. Chem.* **1975**, *47*, 2208. (b) Shoen, G. *Surf. Sci.* **1973**, *35*, 96. (c) Larson, P. E. *J. Electron Spectrosc.* **1974**, *4*, 213.

(15) Bensebaa, F.; Zhou, Y.; Deslandes, Y.; Kruus, E.; Ellis, T. H. *Surf. Sci.* **1998**, *405*, L472.

(16) (a) Shoen, G. *J. Electron Spectrosc. Relat. Phenom.* **1973**, *1*, 377. (b) Hashemi, T.; Hogarth, G. A. *Electrochim. Acta* **1988**, *33*, 1123. (c) Moulder, J. F.; Stickle, W. F.; Sobol, D. E.; Bomben, K. D. In *Handbook of X-ray Photoelectron Spectroscopy*; Chastain, J., Ed.; Perkin-Elmer Corporation, MN, 1992.

(17) Valiokas, R.; Svedhem, S.; Svensson, S. C. T.; Liedberg, B. *Langmuir* **1999**, *15*, 3390.

(18) Bradley, J. S. In *Clusters and colloids*; Schmid, G., Ed.; VCH: Weinhein, Germany, 1994; pp 459−544.

(19) Edwards, P. P. *Mater. Res. Soc. Symp. Proc.* **1992**, *272*, 311.

(20) Nuzzo, R. G.; Dubois, L. H.; Allara, D. L. *J. Am. Chem. Soc.* **1990**, *112*, 558

(21) Badia, Gao, W.; Singh, S.; Dmers, L.; Cuccia, L.; Reven, L. *Langmuir* **1996**, *12*, 1262.

(22) Voicu, R.; Badia, A.; Morin, F.; Lennox, R. B.; Ellis, T. H. *Chem. Mater.* **2000**, *12*, 2646.